WIDE–BAND NONLINEAR CHIRP TRANSDUCERS FOR PLANAR ACOUSTOOPTIC DEFLECTORS

K. Anemogiannis[+], P. Russer[*], R. Weigel[*]

[+]Siemens Research Laboratories München,
Otto–Hahn–Ring 6, D–8000 München 83, FRG
[*]Lehrstuhl für Hochfrequenztechnik, Technische Universität München,
Arcisstr. 21, D–8000 München 2, FRG

ABSTRACT

Design, fabrication and performance characteristics of $LiNbO_3$–based wide–band nonlinear interdigital chirp transducers are reported. A 54 % bandwidth centered at 720 MHz has been obtained for a collinear deflector on a YX substrate. A 66 % bandwidth at a midband frequency of 600 MHz has been designed for a Bragg deflector on a YZ substrate with electrodes tilted to satisfy the Bragg condition. Both tranducers are down–chirp designs. The chirp waveform has been optimized using an accurate model of analysis. The transducers have been fabricated using 10:1 reduction projection printing and liftoff technique. Good agreement has been found between theory and measurement. No severe bulk wave generation has been observed.

INTRODUCTION

Planar acoustooptic deflection results when a surface acoustic wave (SAW) propagates in an optical planar waveguide, producing a periodic variation of the refractive index changes via the photoelastic effect. This provides a moving phase grating which can diffract guided light waves. Planar acoustooptic deflectors can be divided into coplanar guided–to–guided mode coupling (Bragg cells) and collinear coupling of guided waves with radiation modes (substrate deflectors) /1/. In recent years both types of deflectors have been demonstrated to perform the central function incorporated in many planar wave–guide optical signal processing and communication systems /2/. The total number of resolvable spots, according to the Rayleigh criterion, is given by the bandwidth and the transit time of the SAW. As the transit time is limited in both cases, a wide–frequency bandwidth is a highly desirable attribute of a deflector. The bandwidth is restricted by the limited frequency response of the interdigital transducer (IDT), the frequency–dependent overlap of the SAW to the inhomogeneous transverse–optical–mode distribution, and (in the case of a Bragg cell) by the acoustooptic–bandwidth associated with the well–known Bragg phase–matching condition. By choosing an appropriate frequency band and (in case of a Bragg cell) tilting either the entire IDT or the individual electrode fingers to the Bragg angle, the primary limiting factor is the bandwidth of the IDT. A wide transducer bandwidth is achieved by spacing the electrode fingers according to a nonlinearly varying (chirp) synchronous frequency. A flat amplitude response can be obtained without apodization, if a proper chirp law is used. Design considerations for wide–band chirp transducers have been published in the past /3, 4/, however, the requirements for SAW transducers used as part of acoustooptic deflectors are somewhat different. The design parameters for acoustooptic applications are mainly wide bandwidth, flat frequency response, rectangular radiation profile, large aperture, and low insertion loss. In what follows, two very wide–band $LiNbO_3$–based nonlinear chirp transducers are presented. IDT #1 was designed to operate with a 400 MHz bandwidth at a 720 MHz center frequency as part of a collinear substrate deflector on a YX $LiNbO_3$ substrate. IDT #2 was developed for a 400 MHz bandwidth and a midband frequency of 600 MHz as part of a Bragg cell on a YZ $LiNbO_3$ substrate. Both IDTs are down–chirp designs.

TRANSDUCER DESIGN

We first define some basic parameters. Let the chirp waveform v(t), representing the impulse response of the transducer, be given by

$$v(t) = a(t)\cos[\phi(t)]\,, \qquad (1)$$

where $\phi(t)$ is the time–domain phase and the envelope a(t) is zero outside the time intervall $-T/2 \le t \le +T/2$ with T as the length of the waveform. The differential of $\phi(t)$, which is a monotonic function of time t, is the instantaneous frequency f(t), so that

$$f(t) = \frac{d\phi(t)}{2\pi dt}\,. \qquad (2)$$

The frequency f(t) is the *frequency* of the waveform at time t. Defining the chirp rate $\mu(t)$ as the rate of change of instantaneous frequency, expressed in units of Hz/sec, we get

$$\frac{\partial^2\phi(t)}{\partial t^2} = 2\pi\mu(t)\,, \qquad (3)$$

where waveforms with $\mu(t) < 0$ are called down–chirps, while those with $\mu(t) > 0$ are called up–chirps. In order to design a transducer geometry having an impulse response according to equation (1), the electrode positions x_n are given by

$$\phi(x_n/v) = n\pi, \qquad (4)$$

where v is the effective wave velocity in the transducer region.

When piezoelectric Rayleigh waves are generated by IDTs, some excitation of bulk waves is nearly always present. Usually, the degradation of device performance is not severe, but in the case of very wide–band IDTs, the generation of acoustic bulk waves can be the bandwidth limiting factor. To first order each electrode can be regarded as a source of spurious bulk waves with velocity v_b (as well as surface waves with velocity $v < v_b$). This direct generation of bulk modes limit the fractional bandwidth to

$$b_{max} = 2\,\frac{1 - v/v_b}{1 + v/v_b}\,. \qquad (5)$$

While direct generation of bulk waves imposes a limit of approximately 50 %, conversion of piezoelectric Rayleigh waves to bulk waves by interaction within the IDT can be the stronger limiting factor. The phenomenon is significant when the SAW frequency f is greater than $2f'/(1 + v/v_b)$, i.e. in an up–chirp transducer. Here, f' is the local synchronous frequency of the IDT. This effect can only be avoided by restriction of the fractional bandwidth to below about 20 %. On high–coupling substrates like $LiNbO_3$ used for wide–band IDTs, electrode reflections (i) introduce acoustic directionality, which causes dispersive down–chirp transducers to have lower insertion loss than up–chirp configurations; and (ii) contribute additional passband ripple /5/. Hence, limitation of bandwidth imposed by surface–to–bulk mode conversion and insertion loss due to directionality lead to the use of down–chirp transducers for acoustooptic applications.

The aperture of the transducer is fixed by acoustooptic considerations, fabrication restrictions, and the tolerable ohmic losses of the electrodes. The required number of electrodes N is determined by the impedance required. However, internal reflection effects increase with increasing N, so that an optimum value of N must be chosen to obtain both low insertion loss and flat passband shape.

To achieve a flat amplitude response without apodization, phase weigthing, i.e. shaping of the chirp rate $\mu(t)$ is necessary. The design of the transducer starts with the synthesis of a linear frequency–modulated (FM) chirp structure using the impulse model, in which the charge distribution on the electrodes is approximated by δ–function sources located at the electrode centers. The electrode positions are determined assuming a linear chirp waveform given by a quadratic time–domain phase

$$\phi(t) = 2\pi\,(f_0 t \pm \mu t^2/2)\,, \qquad (6)$$

where f_0 is the midband frequency and the chirp rate is a constant given by $\mu = B/T$ with bandwidth B and time dispersion T. Let the chirp waveform of equation (1) (with $a(t) = 1$) be the impulse response of the IDT and denote the Fourier transform of v(t) with $H_0(f)$. Using a sophisticated model, we calculate the frequency response $H_1(f)$, which varies approximately to the 3/2 power of f. In order to obtain a flat passband shape, we first calculate the ratio $H_0(f)/H_1(f) = W(f)$. Usually, W(f) is a high ripple function, so that some smoothing is necessary. Denoting the smoothed spectral weighting function with W'(f), the corrected frequency response is given by $H_0'(f) = W'(f)H_0(f)$. The impulse response $h_0'(t)$, which is the inverse Fourier transform of $H_0'(f)$, gives the positions x_n along the x axis of the electrode centers of the phase–weighted IDT. Adjacent electrodes are excited in a plus–minus fashion. Repeating the described procedure in an iterative manner, the optimum spectral weighting function W'(f) for a required passband shape can be obtained.

MODELLING

The impulse model mentioned above gives a straightforward approximate IDT analysis. Despite being over–simplified, this model illustrates some important features directly and therefore, we use it as an initial model for starting IDT synthesis. However, the impulse model fails to account for a number of second order effects that are often significant in practice. For example, the longitudinal charge distribution on the electrodes, external circuit effects, electrode interactions, reflections and so on are neglected. Our model accounts for most of the important second order effects.

The IDT is split up into a series of basic cells in longitudinal direction which replace the distributed electrical and mechanical phenomena by equivalent network models, so that the response of a complex transducer can be evaluated by analysing an array of networks, using conventional network analysis. Three types of basic cells describing (i) the piezoelectric excitation; (ii) repetitive discontinuities of the mechanical and electrical impedances; and (iii) delay lines are incorporated in the network models. Each of the basic cells is described by a three–port with two acoustic ports and one electric port. Hence, the corresponding hybrid matrix representation is closely related to the physics of the phenomena. The total IDT is composed by cascading the acoustic ports, described by their acoustic wave amplitudes, and connecting the electric ports, described by their electric admittances, in parallel, so that efficient and economical computer analysis is possible.

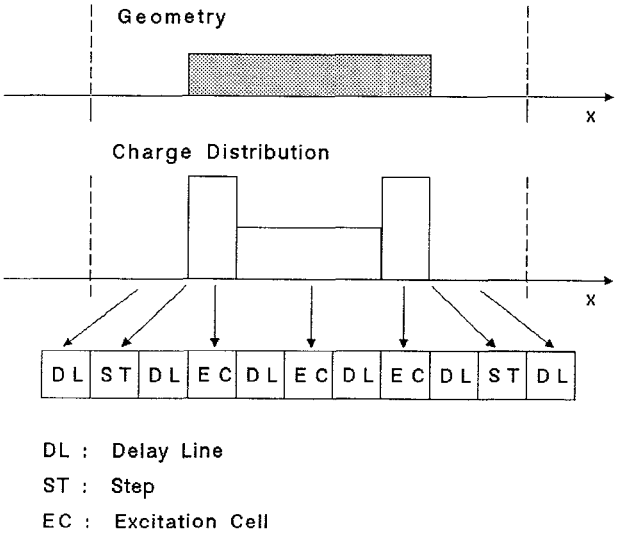

Figure 1 Transducer Basic Cell Model

A Green's function method is used to evaluate the exact longitudinal electrostatic charge distribution /6/. Each electrode is divided into a number of substrips with different widths where the mean charge densities for each substrip are approximated by rectangular pulses using the method of moments /7/. Step discontinuity cells account for electrical and mechanical interactions at the electrode edges as well as for reflection, regeneration and energy storage /8/. Delay line cells simulate wave propagation effects on the free and the metallized regions of the IDT including propagation losses /9/. An illustration of the model is shown in Figure 1.

Furthermore, ohmic losses and losses due to bulk wave generation are included in a heuristic manner. The model is a one–dimensional one, and therefore two–dimensional second–order effects such as diffraction and transverse charge distribution are not taken into account. Their contribution, however, can be safely neglected due to the large transducer apertures.

FABRICATION AND EXPERIMENTAL RESULTS

To fabricate the IDTs, use is made of a standard photolithographic process of the type developed for generating microstructures for VLSI circuits with 10:1 reduction projection printing and liftoff technique. With this process, which has a linewidth resolution of about 0.8 μm, IDT electrodes are fabricated with high precision of the period and high reproducibility of the fingerwidth.

Two transducers have been fabricated on titanium diffused $LiNbO_3$ (Ti:$LiNbO_3$) planar optical waveguide substrates /10/. IDT #1 operates as part of a collinear substrate deflector on YX–$LiNbO_3$, while IDT #2 is designed for Bragg cell applications on YZ–$LiNbO_3$. Both transducers are down–chirp designs. While YZ $LiNbO_3$ is a well known substrate and material orientation in SAW filter technology, YX $LiNbO_3$ up to now has not been studied systematically. Thus, we firstly examined bulk wave generation on YX $LiNbO_3$ by calculating and measuring the impulse response of IDTs with theoretical bandwidths of about 100 %. We found, that the practical bandwidth is limited to about 54 % due to the fact that the longitudinal bulk wave degrades the performance severely at a higher bandwidth.

The design parameters of IDT #1 are given in Table 1. The finger width is varying from about 1 μm to 1.8 μm.

Propagation direction	X	Y
Center frequency f_0 [MHz]	720	600
Bandwidth B/f_0 [%]	54	66
TB–product	59.6	200
Number of electrodes N	195	500
Aperture w [mm]	2.0	0.55
Metallization thickness h [nm]	100	100
Metallization ratio η	0.5	0.5

Table 1 Design Parameters of the Transducers

The theoretical frequency response is shown in Figure 2. The frequency response has been measured by detecting the excited SAW with a two–finger IDT in a distance of 2 mm with an HP8510B network analyzer. This technique is more convenient than direct optical probing of the SAW. Thus, due to the static capacitance of the receiving IDT, the frequency dependence of the filter transfer function must have a linear passband tilt with increasing frequency which is given by the theoretical curve in Figure 3, which also shows the experimental curve. However, one has to remember, that the theoretical electroacoustic transfer function is flat over the passband. Both the IDTs are unmatched and the insertion loss is mainly due to the receiving IDT. As can be seen in Figure 3, there is an excellent agreement both in the bandwidth and the passband shape.

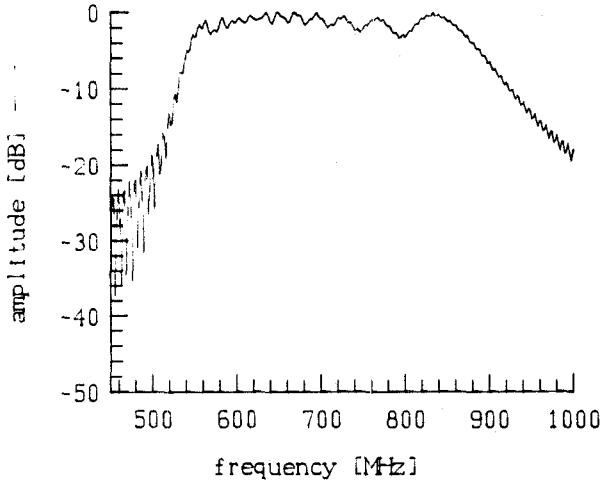

Figure 2 Calculated Electroacoustic Frequency Dependence of IDT #1

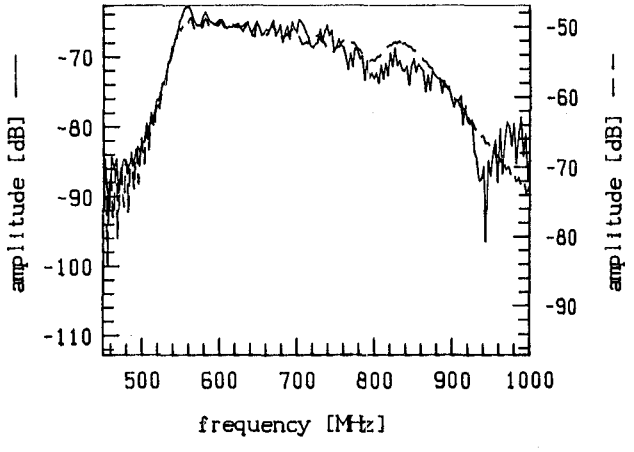

Figure 3 Theoretical (– – – –) and Experimental (————) Frequency Response of the Filter IDT #1

The measured impulse response is shown in Figure 4. The range from 0.53 μs to 0.68 μs exactly represents the SAW and corresponds to the transducer–time dispersion of 0.15 μs. No severe peaks corresponding to bulk waves are found. The peaks at t = 0 and t = 1.335 μs come from the electromagnetic feedthrough between the two IDTs.

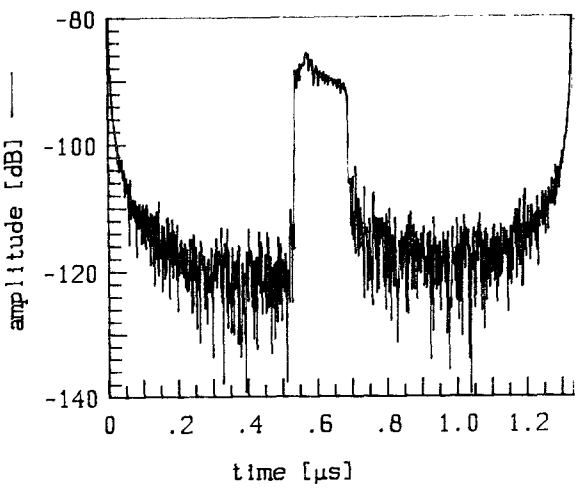

Figure 4 Experimental Impulse Response of the Filter IDT #1

The design parameters of IDT #2 are given in Table 1, too. The electrodes are smoothly tilted in order to maintain the proper Bragg angle between the SAW and the optical beam over the entire IDT bandwidth. Again, good agreement has been found between theory and measurement. The deviation in the insertion loss in this case is only 2 dB. No severe bulk wave generation has been observed.

CONCLUSION

The design and fabrication of wide–band $LiNbO_3$––based nonlinear chirp transducers have been described. A theoretical feasibility of wide bandwidth operation is indicated by the results obtained with the presented model of analysis. The transducer geometries are particularly suited for planar acoustooptic deflectors on Y–cut $LiNbO_3$.

ACKNOWLEDGEMENTS

The authors are most grateful to Dr. G. Riha of Siemens Research Laboratories München for many helpful discussions. Special thanks go to H. Zottl and B. Kamp for the fabrication of the devices. This work has been supported by the Deutsche Forschungsgemeinschaft, Bonn, Federal Republic of Germany.

REFERENCES

/1/ R. Weigel, "Planar acoustooptic interactions in lithium niobate," Proc. International Conference on Nonlinear Optics (NLO '88), Cong, Ireland, 1988, pp. 124–136

/2/ T. Suhara , H. Nishihara, "Integrated optics components and devices using periodic structures," IEEE J. Quantum Electron., vol. QE–22, no. 6, 1986, pp. 845–867

/3/ D.P. Morgan, D.H. Warne, P.N. Naish, D.R. Selviah "Monolithic SAW convolvers using chirp transducers," IEEE Ultrasonics Symp. Proc. 1981, pp. 186–191

/4/ P. Dufilie, "SAW delay line with greater than 100% fractional bandwidth," IEEE Ultrasonics Symp. Proc. 1984, pp. 26–29

/5/ B. Lewis, R.G. Arnold, "Electrode reflections, directionality, and passband ripple in wideband SAW chirp filters," IEEE Trans. Sonics Ultrasonics, vol. SU–32, no. 3, 1985, pp. 409–422

/6/ R. Milsom, N.H.C. Reilly, M. Redwood, "Analysis of generation and detection of surface and bulk acoustic waves by interdigital transducers," IEEE Trans. Sonics Ultrasonics, vol. SU–24, no. 3, 1977, pp. 147–166

/7/ A.R. Baghai–Wadji, O. Männer, R. Ganß–Puchstein, " "Analysis and measurement of transducer end radiation in SAW filters on strongly coupling substrates," IEEE Trans. Microwave Theory Tech., vol. 37, no. 1, 1989, pp. 150–158

/8/ P.V. Wright, H.A. Haus, "Theoretical analysis of second–order effects in surface–wave gratings," Proc. 34th Annual Frequency Control Symposium, Ft. Monmouth, USA, 1980, pp. 262–268

/9/ D.P Morgan, Surface–Wave Devices for Signal Processing. Amsterdam: Elsevier, 1985, pp. 144––145

/10/ A. Rasch, M. Rottschalk, W. Karthe, "Suppression of outdiffusion in Ti:$LiNbO_3$," J. Opt. Commun., vol. 6, no. 1, 1985, pp. 14–17